Current Applied Physics 20 (2020) 43–48

Contents lists available at ScienceDirect

Current Applied Physics

journal homepage: www.elsevier.com/locate/cap

Radial heterostructure and interface effects on thermoelectric transport properties of Bi/Sn and Bi/Sb core/shell nanowires

Hongjae Moon[a,1], Jeongmin Kim[a,1], Dong Won Chun[b], Seokkyoon Hong[a], Young Soo Yoon[c,**], Wooyoung Lee[a,*]

[a] Department of Materials Science and Engineering, Yonsei University, 50 Yonsei-ro, Seodaemoon-gu, Seoul, 03722, Republic of Korea
[b] Advanced Analysis Center, Korea Institute of Science and Technology, Hwarang-ro 14-gil, Seongbuk-gu, Seoul, 02792, Republic of Korea
[c] Department of Materials Science and Engineering, Gachon University, Seongnam-si, 13120, Republic of Korea

ARTICLE INFO

Keywords:
Core/shell nanowires
On-film formation of nanowires
Heterostructure
Interface
Thermoelectric
Seebeck coefficient

ABSTRACT

The thermoelectric transport properties of Bi/Sn and Bi/Sb core/shell (C/S) nanowires grown by the method of on-film formation of nanowires were systematically investigated. The electrical conductivity and Seebeck coefficient of nanowires with different diameters were measured as a function of the temperature. The contribution of Sn and Sb shells to the total transport in the C/S nanowires was determined using analytical fitting based on the parallel combination of the conductive system model. The carrier-interface boundary scattering at the C/S interface was quantitatively evaluated as the sheet resistance. In addition, the effect of hole doping on the transport properties was also observed in the Bi/Sn C/S nanowires.

1. Introduction

The thermoelectric performance of a material is evaluated using the dimensionless thermoelectric figure of merit ($ZT = \sigma S^2 T/\kappa$), which can be enhanced by optimization of electrical conductivity (σ), Seebeck coefficient (S), and thermal conductivity (κ) at a temperature (T) [1]. However, simultaneous optimization is challenging because it is very difficult to control the three interrelated thermoelectric properties independently [2]. To increase ZT, nanostructures have been intensively investigated via two different routes. First, the reduction in the thermal conductivity was successfully demonstrated by phonon engineering in nanostructures. The classical size effect caused by a spatial restriction in nanowires effectively decreases the phonon mean free path through the phonon-surface boundary scattering [3–8]. In addition, the modification of hetero-nanostructures inside nanowires such as alloying, embedding nanoparticles, and using superlattice or core/shell (C/S) has further efficiently suppressed phonon transport by the phonon-interface boundary scattering [9–13]. For an approach similar to that involving the phonon-surface/interface scattering, holey structures were extensively studied in nanoribbons [14,15]. The second route is the enhancement of the thermoelectric power factor (σS^2), which indicates the electrical thermoelectric performance of a material. After the first theoretical study predicting the increase in the power factor due to the quantum confinement effect in low-dimensional materials [16,17], the energy band engineering and optimization of thermoelectric properties for the power factor enhancement were demonstrated using various nanowires [8,18,19]. Moreover, the energy filtering effect through the hetero-nanostructure modification has effectively improved the thermoelectric performance [20–23]. The C/S heterostructure is another promising nanostructure for power factor enhancement and phonon engineering [13,24]. In the previous study on semimetal/semiconductor Bi/Te C/S nanowire, it was found that the decrease in the crystal anisotropy due to the lattice mismatch between the core and shell can enhance the Seebeck coefficient because of the crystal-structure-sensitive energy band in the semimetal [24]. In the Bi/Te C/S nanowire, however, it is difficult to observe the interaction of the transport phenomena between the core and shell such as the interface effect, because the effect of the semimetallic Bi core is dominant on the overall properties of the C/S nanowire [24]. This is because the conductance of the semiconducting shell is significantly smaller than that of core; therefore, it is important to select materials with comparable conductance to better understand the interaction between the core and shell of the conductive C/S structure. In the present work, we studied the thermoelectric transport properties of Bi/Sn and Bi/Sb C/S

* Corresponding author.
** Corresponding author.
E-mail addresses: benedicto@gachon.ac.kr (Y.S. Yoon), wooyoung@yonsei.ac.kr (W. Lee).
[1] Hongjae Moon and Jeongmin Kim contributed equally to this work.

https://doi.org/10.1016/j.cap.2019.10.007
Received 30 April 2019; Accepted 7 October 2019
Available online 07 October 2019

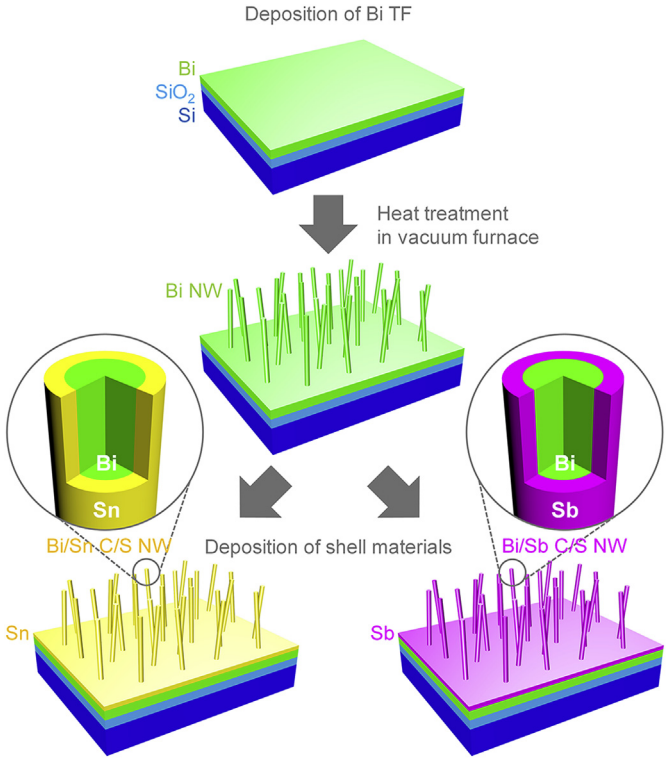

Fig. 1. Schematic representations of Bi/Sn and Bi/Sb core/shell (C/S) nanowires prepared by the on-film formation of nanowires (OFFON) method. (Step 1) A Bi film was deposited on a thermally oxidized Si substrate using a sputtering system. (Step 2) Bi nanowires were grown on the Bi film during the heat treatment in a vacuum furnace. (Step 3) The Sn and Sb shell were deposited on the as-grown Bi nanowires on the substrate using a sputtering system.

nanowires grown by the method of on-film formation of nanowires (OFFON). The electrical conductivity and Seebeck coefficient were measured as a function of the temperature and diameter, and the shell-dependent transport properties were systematically investigated with the interface effect.

2. Materials and methods

2.1. Sample preparation and characterization

Bi/Sn and Bi/Sb C/S nanowires were fabricated by annealing and post-deposition processes, as shown in Fig. 1. The single-crystalline Bi nanowires were prepared as the core of samples by the OFFON method [13,25]. Bi films (< 50 nm) were deposited on a thermally oxidized Si (100) substrate using an ultrahigh-vacuum (UHV) radio-frequency (RF) sputtering system. The Bi nanowires were grown on the Bi film during the heat treatment (5 h at 250 °C) in an UHV furnace, to release thermal stress due to the thermal expansion mismatch between the Bi film and substrate [25]. The Sn and Sb shells (~20-nm thickness) were subsequently deposited on the as-grown Bi nanowires substrates using the UHV RF sputtering system for the Bi/Sn and Bi/Sb C/S nanowires, respectively. The three steps were conducted in situ under a high vacuum (10^{-7} Torr) condition to inhibit oxidation.

The structure and chemical composition of the C/S nanowires were confirmed by scanning transmission electron microscopy (STEM) and energy dispersive X-ray spectroscopy (EDS), as shown in Fig. 2. Although the high-angle annular dark field (HAADF) STEM images (Fig. 2a and e) show that the Sn shell surface is slightly rougher than the Sb shell surface, the EDS results reveal that the smooth surface of Bi cores (Fig. 2c and e) were entirely covered by the shell materials in both C/S nanowires (Fig. 2b, d, f, and h). Moreover, the uniformity of the nanowire diameter was confirmed, and the average shell thickness was found to be about 20 nm for both C/S nanowires.

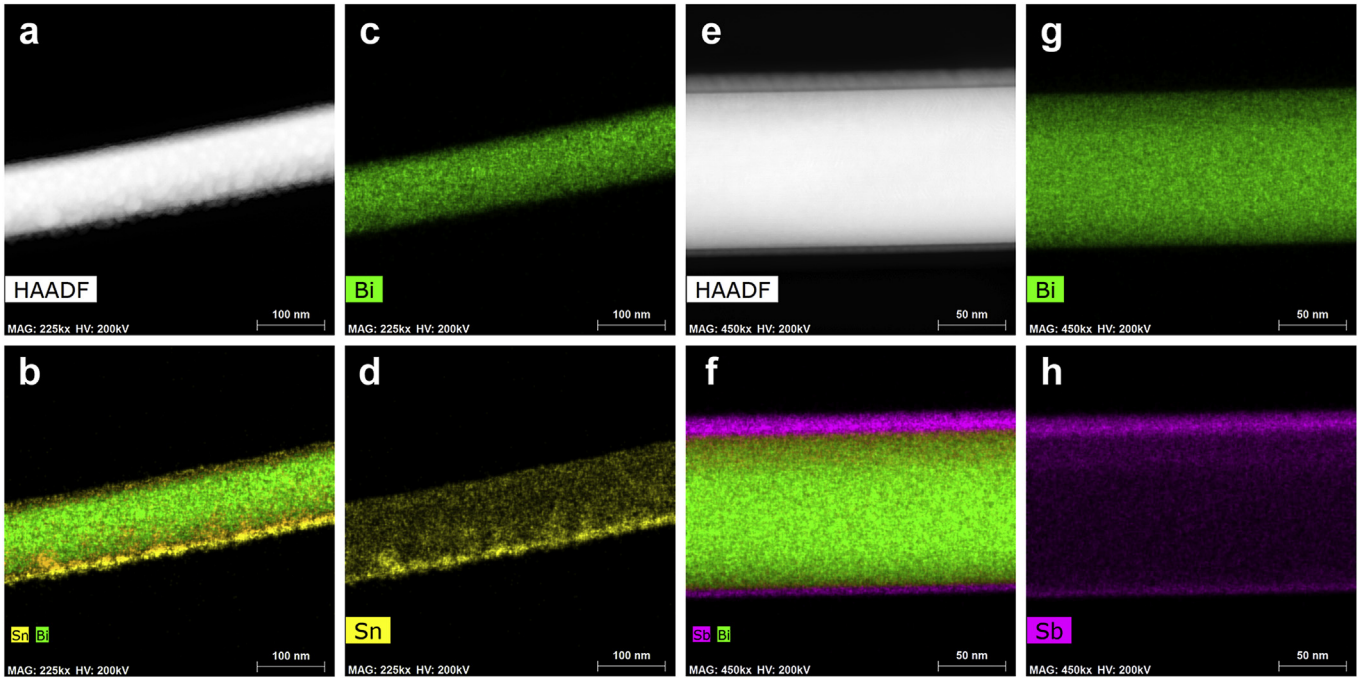

Fig. 2. Spatial distribution of elements on Bi/Sn and Bi/Sb C/S nanowires. a, e. High-angle annular dark field (HAADF) scanning transmission electron microscopy (STEM) images of Bi/Sn and Bi/Sb C/S nanowires. b, f. Energy dispersive X-ray spectroscopy (EDS) mapping images of Bi/Sn and Bi/Sb C/S nanowires. c, g. Element maps of Bi core (green). d, h. Element maps of Sn (yellow) and Sb (purple) shells, respectively. (For interpretation of the references to colour in this figure legend, the reader is referred to the Web version of this article.)

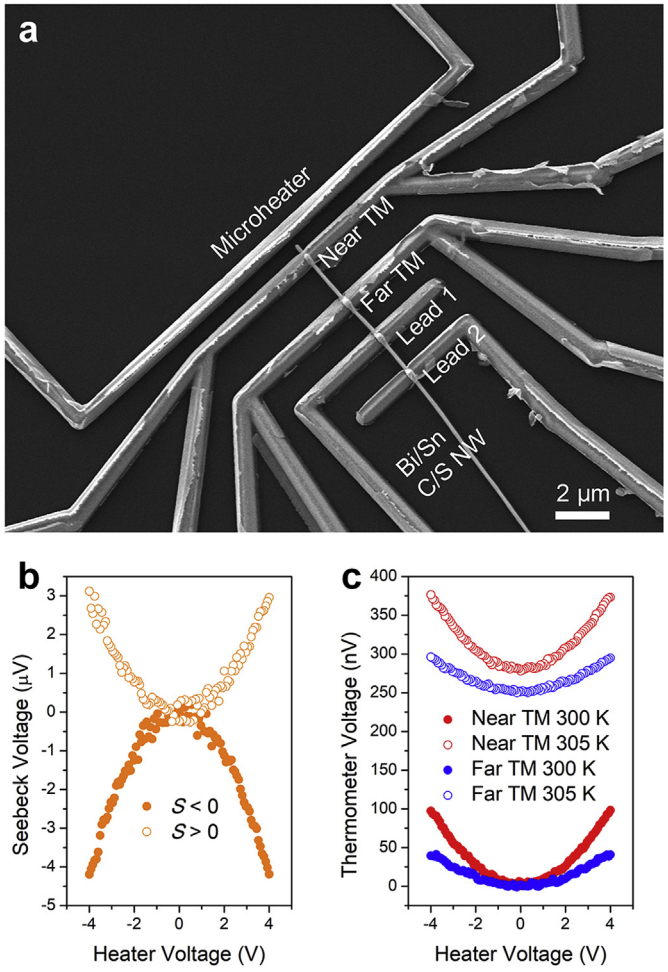

Fig. 3. Device fabrication and measurements. a. Scanning electron microscopy (SEM) image of a single nanowire thermoelectric device. b. Positive and negative Seebeck voltages with respect to the heater voltage. c. Thermometer (TM) voltages of near and far TMs at two different system temperatures.

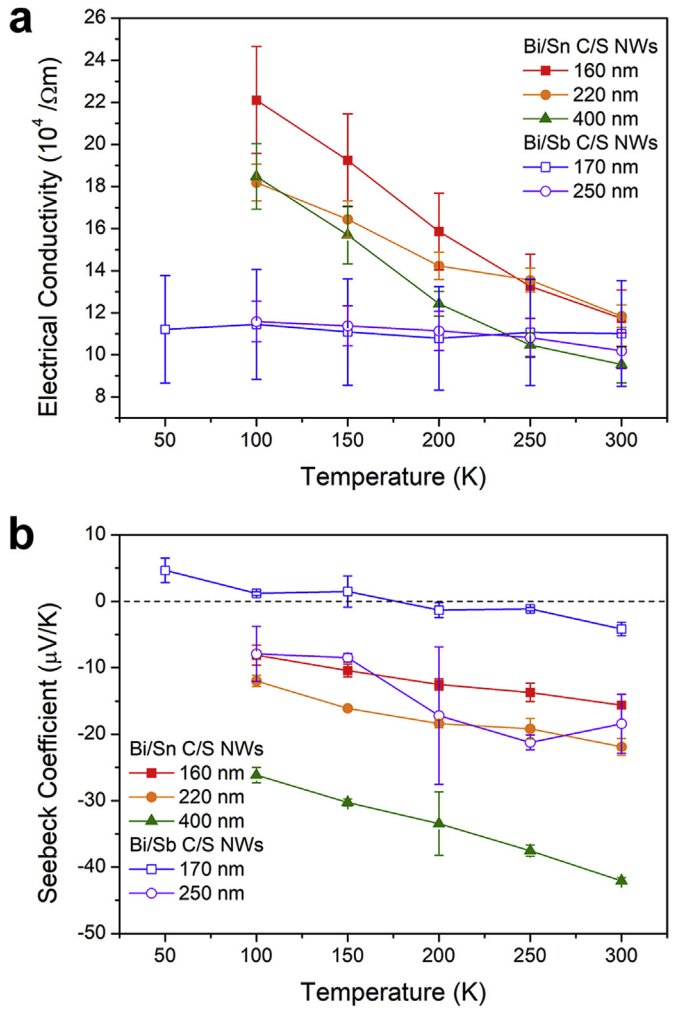

Fig. 4. Temperature-dependent transport properties of Bi/Sn and Bi/Sb C/S nanowires. a. Electrical conductivity and b. Seebeck coefficient obtained as a function of the temperature for different diameters.

2.2. Device fabrication and measurement

Fig. 3a shows a scanning electron microscopy (SEM) image of a thermoelectric device based on an individual C/S nanowire for the electrical conductivity and Seebeck coefficient measurements. The device has a microscale heater and two-different microscale thermometers for Seebeck coefficient measurements and two resistance leads for the four-terminal measurement. These Cr/Au (5/200 nm) electrodes were defined and deposited by using typical electron-beam lithography and the UHV sputtering system, respectively, on the SiO_2/Si substrate with the dispersed C/S nanowires. To obtain the direct electrical contact between the electrodes and Bi core, Ar plasma etching was conducted before the deposition [26].

The electrical conductivity of the single C/S nanowire was measured using the four-different electrodes (thermometers and leads) based on the four terminal measurement technique to prevent a deviation due to the contact resistance. For the Seebeck coefficient measurement, the Joule heating through the micro heater generated an in-plane temperature gradient on the substrate, and the two thermometers were used to measure the voltages and temperature differences (ΔV and ΔT, respectively). The Seebeck voltage (ΔV) was proportional to the square of the heater voltage in the case of Joule heating ($P = V^2/R$), and the sign of Seebeck coefficient could be determined from the shape of the parabolic curve, as shown in Fig. 3b. To obtain the temperature difference (ΔT), the resistance change of each thermometer was precisely measured using a Lock-in amplifier as a voltage signal (Fig. 3c). The parabolic thermometer voltages could be converted to temperatures according to the temperature coefficient of resistance (TCR) obtained at the different system temperatures. Finally, the Seebeck coefficient was calculated using the relation $S = \Delta V/\Delta T$. The details of the device fabrication and measurement technique are presented in Ref. [8].

3. Results and discussion

3.1. Temperature-dependent transport properties

Fig. 4 shows the temperature-dependent electrical conductivity and Seebeck coefficient of Bi/Sn and Bi/Sb C/S nanowires. In the previous study on pure Bi nanowires, it was found that the temperature dependence of electrical conductivity gradually changes from semiconducting to metallic as increasing diameter due to the reduction of surface carrier scattering and thus pure Bi nanowires with diameters larger than 100 nm exhibit the metallic dependence [8]. Therefore, the electrical conductivity of Bi/Sn C/S nanowires consisting of a metallic shell increases with decreasing temperature (Fig. 4a). On the other hand, in the case of Bi/Sb C/S nanowires, the temperature dependence is hardly observed, and this is likely due to the effect of the Sb shell because both C/S nanowires have the same Bi core. The details of the shell effect on the overall nanowire will be discussed below.

The Seebeck coefficient of the C/S nanowires is also affected by the

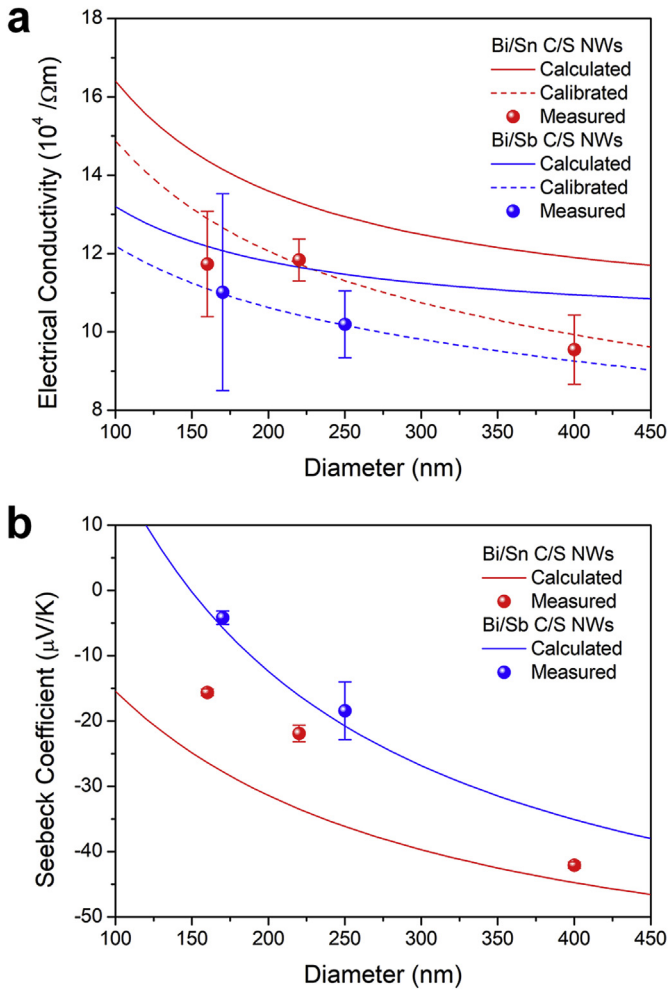

Fig. 5. Diameter-dependent transport properties of Bi/Sn and Bi/Sb C/S nanowires. a. Electrical conductivity and b. Seebeck coefficient represented as a function of the diameter. The measured data (solid circles) was fitted by a parallel combination of conductive system model with (dashed lines) and without (solid lines) the interface effect.

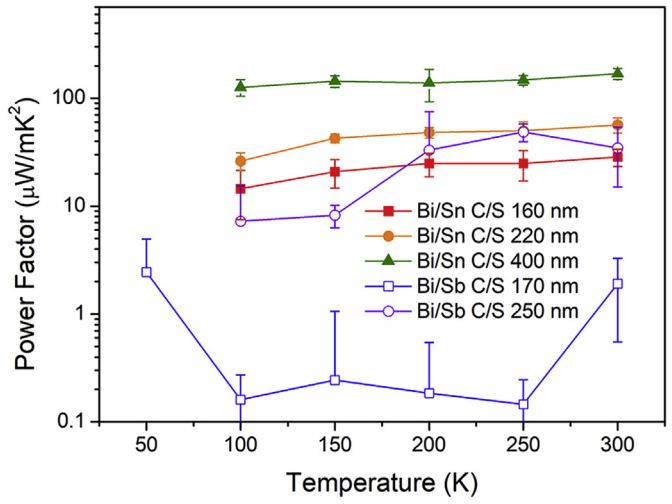

Fig. 6. Thermoelectric power factor of Bi/Sn and Bi/Sb C/S nanowires. The power factor was calculated using the thermoelectric properties measured with respect to the temperature for different diameters.

transport properties of the shell. For the Bi/Sn C/S nanowires, the Seebeck coefficient monotonically decreased with decreasing temperature, which is consistent with the trend observed for the Seebeck coefficients of pure Bi nanowires (Fig. 4b) [8]. This temperature dependency was also evident in the Bi/Sb C/S nanowire with a 250-nm diameter. In the case of 170-nm Bi/Sb C/S, however, the values were significantly smaller than that of other nanowires. Moreover, the Seebeck coefficient changed almost linearly from a negative value to a positive value with decreasing temperature. This temperature dependence can also be considered to be the influence of the properties of the Sb shell having a positive Seebeck coefficient, but further quantitative analysis was conducted to determine the contribution of the core and shell to the overall properties, as discussed below.

3.2. Diameter-dependent transport properties

Fig. 5 shows the diameter-dependent electrical conductivity and Seebeck coefficient of Bi/Sn and Bi/Sn C/S nanowires at 300 K. To confirm the contribution of the core and shell to the total transport properties, the measured diameter-dependent electrical conductivity and Seebeck coefficient were fitted by a parallel combination of a conductive system model, which can be expressed as

$$\sigma_{total} = \frac{A_{core}\sigma_{core} + A_{shell}\sigma_{shell}}{A_{total}}, \quad (1)$$

$$S_{total} = \frac{G_{core}S_{core} + G_{shell}S_{shell}}{G_{total}}, \quad (2)$$

where σ, A, S, and G are the electrical conductivity, cross-sectional area, Seeebck coefficient, and electrical conductance, respectively [26]. As shown in Eqs. (1) and (2), the total transport properties can be determined from the partial properties of the core and shell with weighting factors. The weighting factors for the partial electrical conductivity and partial Seebeck coefficient are the cross-sectional area and electrical conductance, respectively.

As shown in Fig. 5a, the total conductivity slightly increased with the decreasing diameter, which indicates that the shell is more conductive than the core. According to the previous study on pure Bi nanowires (core), the diameter dependence of the electrical conductivity was no longer observed when the diameter increases above 100 nm [8], and the thickness of the shell was not varied in this study. Therefore, with decreasing diameter, the contribution of the shell increases due to the increase in the weighting factor (cross-sectional area). Although, the calculations (solid lines) based on Eq. (1) clearly demonstrated the diameter dependence of the electrical conductivity, the values were slightly larger than the measured conductivity. This overestimation in the case of Eq. (1) can be attributed to the additional carrier scattering at the interface between the core and shell [27–29]. This interface effect was not considered in the parallel combination of the conductive system model, and thus, to calibrate the interface scattering effect, the interface resistance was introduced into Eq. (1) as the series combination. As shown by the dashed lines in Fig. 5a, the calibrated conductivities were in good agreement with measured values, and the interface resistance was found to correspond to a sheet resistance of 15 Ω/sq for both C/S nanowires. However, even with the interface effect, there were slight differences between the measured and calibrated conductivities for the Bi/Sn C/S nanowires. This can be explained by the effect of hole doping on the Bi core due to the Sn shell. Sn atoms in Bi cause *p*-type doping by depriving the valence electrons of Bi [30]. Since the carrier mobility of holes is lower than that of electrons in Bi, *p*-type doping decreases the electrical conductivity [31]. A similar effect was also observed in the Seebeck coefficient as discussed below.

As shown in Fig. 5b, the Seebeck coefficient decreased with the decreasing diameter for both C/S nanowires. As mentioned in the previous section, this behavior is attributed to the increase in the shell contribution due to the reduction in the diameter. The Seebeck

coefficients of Sn and Sb are approximately −1.5 and 50 μV/K, respectively, which are significantly smaller than or opposite in sign compared to that of Bi (~ −65 μV/K) [8,32,33]. Therefore, increasing the contribution of the shell reduces the total Seebeck coefficient to less than the Seebeck coefficient of Bi core. Similarly, it can be explained that the absolute values of the Seebeck coefficient in Bi/Sb C/S nanowires are smaller than those of Bi/Sn C/S nanowires at similar diameters. The diameter dependence was calculated using Eqs. (1) and (2) based on the parallel combination of the conductive system model (solid lines in Fig. 5b). In the case of the Seebeck coefficient, the weighting factor that determines the contribution of the partial Seebeck coefficient is not the electrical conductivity but the conductance. Therefore, the contribution to the total Seebeck coefficient of the interface is negligible because the conductance of the interface is significantly lower than that of the core and shell [26]. As a result, the diameter-dependent Seebeck coefficient could be fitted by Eq. (2) based on the conductance calculation using Eq. (1) without considering the interface effect. The calculated Seebeck coefficient was in good agreement with measured values for the Bi/Sb C/S nanowires. However, an overestimation was observed in the case of Bi/Sn C/S nanowires. This can also be explained by the hole doping effect originating from the Sn shell [26]. The Seebeck coefficient of Bi is extremely sensitive to the carrier concentration, because the semimetallic band structure consisting of indirect conduction and valence bands overlap, which can be expressed as $S = (\sigma_h S_h + \sigma_e S_e)/(\sigma_h + \sigma_e)$, where the subscripts h and e denote "hole" and "electron," respectively. Therefore, a small variation in the carrier concentration induced by the shell can lead to a decrease in the Seebeck coefficient of the Bi core, resulting in a reduction in the total Seebeck coefficient. As a result, the deviation due to the hole doping effect by the Sn shell increases with decreasing diameter.

3.3. Power factor

Finally, the power factor, which indicates the electrical thermoelectric efficiency, was calculated from the measured electrical conductivity and Seebeck coefficient according to the following relationship: power factor = $S^2\sigma$. Fig. 6 shows the power factor as a function of the temperature. In Bi/Sn C/S nanowires, contrasting temperature dependences were observed for the electrical conductivity and Seebeck coefficient (Fig. 4). The power factor exhibited a very weak temperature dependence but it slightly decreased with the temperature owing to S^2. In the case of Bi/Sb C/S nanowires, where the temperature dependence of electrical conductivity is hardly observed, the variation in the Seebeck coefficient directly reflected on the power factor. The power factor of Bi/Sb C/S nanowires is smaller than that of Bi/Sn C/S nanowires with a similar diameter. In particular, the 170-nm-Bi/Sb nanowire exhibited significantly low values, which can be attributed to the transport properties of the Sb shell (which has a Seebeck coefficient sign opposite to that of the Bi). Furthermore, we could not observe the enhancement of the power factor originating from the Bi core revealed in the previous study on Bi/Te C/S nanowires [24], which seems to be due to the influence of the relatively conductive shell on the overall properties.

4. Conclusion

We studied the thermoelectric transport properties of Bi/Sn and Bi/Sb C/S nanowires grown by the OFFON method. The electrical conductivity and Seebeck coefficient were measured as a function of the temperature for both C/S nanowires with different diameters. The contributions of Sn and Sb shells to the total transport in the C/S nanowires were systematically investigated using the temperature- and diameter-dependent transport properties. The transport properties of C/S nanowires were analytically fitted by the parallel combination of the conductive system model. The carrier-interface boundary scattering at the C/S interface was quantitatively evaluated as the sheet resistance. In addition, an effect of hole doping on the transport properties was also observed in the Bi/Sn C/S nanowires. Thus, we present quantitative experimental data on the effect of the structure and interface of C/S nanowires on transport phenomena, and we provide the criteria for shell materials of the C/S structure for thermoelectric applications.

Acknowledgement

This work was supported by the Agency for Defense Development, Republic of Korea (UD170089GD) and the National Research Foundation of Korea (NRF) grant funded by the Korea government (MSIT) (2017R1A2A1A17069528). JK was supported by Basic Science Research Program through the National Research Foundation of Korea (NRF) funded by the Ministry of Education (2019R1I1A1A01063687)

References

[1] H.J. Goldsmid, Thermoelectric Refrigeration, Plenum Press, New York, 1964.
[2] A. Majumdar, Thermoelectricity in semiconductor nanostructures, Science 303 (2004) 777–778.
[3] D. Li, Y. Wu, P. Kim, L. Shi, P. Yang, A. Majumdar, Thermal conductivity of individual silicon nanowires, Appl. Phys. Lett. 83 (2003) 2934–2936.
[4] J. Zhou, C. Jin, J.H. Seol, X. Li, L. Shi, Thermoelectric properties of individual electrodeposited bismuth telluride nanowires, Appl. Phys. Lett. 87 (2005) 133109.
[5] A.I. Boukai, Y. Bunimovich, J. Tahir-Kheli, J.-K. Yu, W.A. Goddard Iii, J.R. Heath, Silicon nanowires as efficient thermoelectric materials, Nature 451 (2008) 168.
[6] A.I. Hochbaum, R. Chen, R.D. Delgado, W. Liang, E.C. Garnett, M. Najarian, A. Majumdar, P. Yang, Enhanced thermoelectric performance of rough silicon nanowires, Nature 451 (2008) 163–167.
[7] E.Z. Xu, Z. Li, J.A. Martinez, N. Sinitsyn, H. Htoon, N. Li, B. Swartzentruber, J.A. Hollingsworth, J. Wang, S.X. Zhang, Diameter dependent thermoelectric properties of individual SnTe nanowires, Nanoscale 7 (2015) 2869–2876.
[8] J. Kim, S. Lee, Y.M. Brovman, P. Kim, W. Lee, Diameter-dependent thermoelectric figure of merit in single-crystalline Bi nanowires, Nanoscale 7 (2015) 5053–5059.
[9] E.K. Lee, L. Yin, Y. Lee, J.W. Lee, S.J. Lee, J. Lee, S.N. Cha, D. Whang, G.S. Hwang, K. Hippalgaonkar, A. Majumdar, C. Yu, B.L. Choi, J.M. Kim, K. Kim, Large thermoelectric figure-of-merits from SiGe nanowires by simultaneously measuring electrical and thermal transport properties, Nano Lett. 12 (2012) 2918–2923.
[10] J.W. Roh, J. Ham, J. Kim, H. Moon, H.S. Kim, W. Lee, Extreme reduction of thermal conductivity by embedding Al2O3 nanoparticles into single-crystalline Bi nanowires, Acta Mater. 136 (2017) 315–322.
[11] D. Li, Y. Wu, R. Fan, P. Yang, A. Majumdar, Thermal conductivity of Si/SiGe superlattice nanowires, Appl. Phys. Lett. 83 (2003) 3186–3188.
[12] J. Kang, W. Shim, S. Lee, J.W. Roh, J.-S. Noh, P.W. Voorhees, W. Lee, Thermodynamic-enabled synthesis of Bi/Bi14Te6 axial heterostructure nanowires, J. Mater. Chem. 1 (2013) 2395–2400.
[13] J. Kang, J.W. Roh, W. Shim, J. Ham, J.-S. Noh, W. Lee, Reduction of lattice thermal conductivity in single Bi-Te core/shell nanowires with rough interface, Adv. Mater. 23 (2011) 3414–3419.
[14] J.-K. Yu, S. Mitrovic, D. Tham, J. Varghese, J.R. Heath, Reduction of thermal conductivity in phononic nanomesh structures, Nat. Nanotechnol. 5 (2010) 718.
[15] J. Tang, H.-T. Wang, D.H. Lee, M. Fardy, Z. Huo, T.P. Russell, P. Yang, Holey silicon as an efficient thermoelectric material, Nano Lett. 10 (2010) 4279–4283.
[16] L.D. Hicks, M.S. Dresselhaus, Effect of quantum-well structures on the thermoelectric figure of merit, Phys. Rev. B Condens. Matter Mater. Phys. 47 (1993) 12727–12731.
[17] L.D. Hicks, M.S. Dresselhaus, Thermoelectric figure of merit of a one-dimensional conductor, Phys. Rev. B Condens. Matter Mater. Phys. 47 (1993) 16631–16634.
[18] P.M. Wu, J. Gooth, X. Zianni, S.F. Svensson, J.G. Gluschke, K.A. Dick, C. Thelander, K. Nielsch, H. Linke, Large thermoelectric power factor enhancement observed in InAs nanowires, Nano Lett. 13 (2013) 4080–4086.
[19] J. Moon, J.-H. Kim, Z.C.Y. Chen, J. Xiang, R. Chen, Gate-modulated thermoelectric power factor of hole gas in Ge–Si core–shell nanowires, Nano Lett. 13 (2013) 1196–1202.
[20] S.C. Andrews, M.A. Fardy, M.C. Moore, S. Aloni, M. Zhang, V. Radmilovic, P. Yang, Atomic-level control of the thermoelectric properties in polytypoid nanowires, Chem. Sci. 2 (2011) 706–714.
[21] T. Zhang, S. Wu, J. Xu, R. Zheng, G. Cheng, High thermoelectric figure-of-merits from large-area porous silicon nanowire arrays, Nano Energy 13 (2015) 433–441.
[22] Z. Xiong, Y. Cai, X. Ren, B. Cao, J. Liu, Z. Huo, J. Tang, Solution-processed CdS/Cu2S superlattice nanowire with enhanced thermoelectric property, ACS Appl. Mater. Interfaces 9 (2017) 32424–32429.
[23] H. Yang, J.-H. Bahk, T. Day, A.M.S. Mohammed, G.J. Snyder, A. Shakouri, Y. Wu, Enhanced thermoelectric properties in bulk nanowire heterostructure-based nanocomposites through minority carrier blocking, Nano Lett. 15 (2015) 1349–1355.
[24] J. Kim, M.-W. Oh, G. Kim, J.-H. Bahk, J.Y. Song, S.G. Jeon, D.W. Chun, J.-H. Bae, W. Shim, W. Lee, Strain-engineered allotrope-like bismuth nanowires for enhanced thermoelectric performance, Acta Mater. 144 (2018) 145–153.
[25] W. Shim, J. Ham, K.I. Lee, W.Y. Jeung, M. Johnson, W. Lee, On-film formation of Bi nanowires with extraordinary electron mobility, Nano Lett. 9 (2009) 18–22.

[26] J. Kim, G. Kim, J.-H. Bahk, J.-S. Noh, W. Lee, Enhanced thermoelectric properties in Bi/Te core/shell heterostructure nanowires through strain and interface engineering, Nano Energy 32 (2017) 520–525.
[27] A. Mavrokefalos, Q. Lin, M. Beekman, J.H. Seol, Y.J. Lee, H. Kong, M.T. Pettes, D.C. Johnson, L. Shi, In-plane thermal and thermoelectric properties of misfit-layered [(PbSe)0.99]x(WSe2)x superlattice thin films, Appl. Phys. Lett. 96 (2010) 181908.
[28] P.P. Wang, X.J. Wang, J.L. Du, F. Ren, Y. Zhang, X. Zhang, E.G. Fu, The temperature and size effect on the electrical resistivity of Cu/V multilayer films, Acta Mater. 126 (2017) 294–301.
[29] P.P. Wang, C. Xu, E.G. Fu, J.L. Du, Y. Gao, X.J. Wang, Y.H. Qiu, The study on the electrical resistivity of Cu/V multilayer films subjected to helium (He) ion irradiation, Appl. Surf. Sci. 440 (2018) 396–402.
[30] H. Jin, B. Wiendlocha, J.P. Heremans, P-type doping of elemental bismuth with indium, gallium and tin: a novel doping mechanism in solids, Energy Environ. Sci. 8 (2015) 2027–2040.
[31] F.Y. Yang, K. Liu, K. Hong, D.H. Reich, P.C. Searson, C.L. Chien, Y. Leprince-Wang, K. Yu-Zhang, K. Han, Shubnikov-de Haas oscillations in electrodeposited single-crystal bismuth films, Phys. Rev. B Condens. Matter Mater. Phys. 61 (2000) 6631–6636.
[32] P. Fiflis, L. Kirsch, D. Andruczyk, D. Curreli, D.N. Ruzic, Seebeck coefficient measurements on Li, Sn, Ta, Mo, and W, J. Nucl. Mater. 438 (2013) 224–227.
[33] G.A. Saunders, C. Miziumski, G.S. Cooper, A. Lawson, The seebeck coefficients of antimony and arsenic single crystals, J. Phys. Chem. Solids 26 (1965) 1299–1303.